

Control of a mechanism for the application of variable axial loads in a multiaxial fatigue testing machine

Luis Paulo Brasil de Souza¹ , Dario Prada Parra¹, José Alan Foicinha Raiol², Arthur Martins Barbosa Braga¹, Leonardo Dantas Rodrigues² 

¹Pontifícia Universidade Católica do Rio de Janeiro, Departamento de Engenharia Mecânica, Laboratório de Sensores a Fibra Óptica. Rua Marquês de São Vicente, 225, Gávea, 22451-900, Rio de Janeiro, RJ, Brasil.

²Universidade Federal do Pará, Departamento de Engenharia Mecânica, Núcleo Avançado de Análise de Tensões. Rua Augusto Corrêa, 01, Guamá, 66075-110, Belém, PA, Brasil.

e-mail: luisbrasil@aluno.puc-rio.br; daprada@puc-rio.br; abraga@puc-rio.br, alan_rayol@hotmail.com; leodr@ufpa.br

ABSTRACT

The loads acting on mechanical components are usually complex, and the more traditional fatigue analysis criteria may be non-conservative, especially in out-of-phase and non-proportional loadings. Many multiaxial fatigue models have been developed and need to be experimentally validated. This work describes the load control mechanism of a low-cost electromechanical multiaxial fatigue testing machine, which applies variable axial and torsional loads. A load cell interconnected to the motor control system was manufactured and instrumented with extensometers. For the axial load, a four-bar mechanism coupled to a power screw was designed to apply alternating axial loads, thus ensuring a higher load frequency and preservation of the motor, which will not need to alternate its direction of rotation. The machine's control system, focused on out-phase loading, is based on the data sent by the load cell and pulse encoders per degree for each motor, ensuring good accuracy in applied loads. Tests were carried out to check the system's response, in which it was possible to apply load curves of torque and axial force in different phase shift angle. Therefore, several existing multiaxial fatigue models can be tested with good reliability.

Keywords: Mechanisms; multiaxial fatigue; out-of-phase loadings; loading control system.

1. INTRODUCTION

Multiaxial fatigue is an important field of research that has been studied extensively in recent years due to its application in various areas of industry [1]. The general characteristics of a typical fatigue failure for macroscopically elastic methods, like the SN method, consisted of two steps: (i) initial damage occurred, produced by a strong cyclic stress, leading to nucleation and crack initiation; and (ii) cyclical and progressive growth of this crack until the component fractures [2]. Therefore, the knowledge of the behavior of mechanical components when manifested to loads of different forms and natures is of great importance to quantify the damage that the component can or will be able to withstand, thus avoiding failure of the same component [3].

An important way to contribute to research in this field is using fatigue testing machines aimed mainly at damage calculation, crack propagation, and service life calculation [4]. There are several approaches and models to calculate the service life or fatigue resistance of an element subjected to multiaxial loads [1, 5]. The high cycle fatigue (HCF) models can be classified according to different criteria, such as: the critical plane-based criterion, the equivalent stress criterion, the stress invariant criterion, and the microscopic integral criterion [6].

The critical plane criterion selects damage parameters on the plane direction of crack initiation and propagation [1, 7]. It is based on the mechanism of fatigue crack initiation and growth and has a certain physical meaning. FINDLEY [8] found that maximum shear stress amplitude is the critical factor for initiating and propagating multi-axial fatigue cracks under bending-torsion loading. The normal stress on the maximum shear stress plane had a greater effect on the growth of cracks, so the plane with the largest linear combination of normal stress and shear stress was used as the critical plane to establish the failure criterion.

The equivalent stress criterion largely used, is based on the static strength theory, and is efficient for proportional loads. The model that was initially formulated by GOUGH and POLLARD [9]. Determined the fatigue limit of various materials under different bending and torsional stresses and provided the maximum tensile stress

test applicable to the failure of metallic materials under bending and torsional loading. GUEST [10] proposed an equivalent parameter and established a criterion based on the maximum shear stress, which in some cases is consistent with the elliptic equation of Gough's criterion.

The stress invariant criterion is a method that directly links fatigue strength to the second invariant of the stress deviator and the first invariant of the stress. However, it cannot differentiate between tensile and compressive stress effects. The models of SINES and OHGI [11], WHITE *et al.* [12], and KAKUNO and KAWADA [13] can be classified in this category and are good examples of this approach.

DANG-VAN *et al.* [14] first proposed the microscopic integral criterion, which suggests that fatigue cracks are generated by the plastic deformation of grains on the slip band. PAPADOPOULOS [15–17] later discovered that the plastic deformation of some grains is caused by components of the shear stress amplitude on any plane for metal materials subjected to cyclic loading.

Multiaxial fatigue, as well as uniaxial fatigue, has analysis methods that take into account the range of stresses, which can be used when no significant plasticity occurs in the object component of analysis, and methods that take into account the range of strains [18]. However, multiaxial fatigue methods are still in full development, serving as motivation for several researchers worldwide. These methods, for the most part, have a strong empirical bias, always requiring experimental tests for validation and adjustment. In general, fatigue tests are costly compared to other mechanical tests due to the high costs of multiaxial fatigue machines, the duration of the tests, and the number of samples, which slows down the advancement of research. The machine proposed was based on SANCHEZ's [19] machine, a biaxial traction-torsion machine that includes the development of the load and torque cell and the implementation of its respective control in order to evaluate models of incremental plasticity in multiaxial fatigue. Furthermore, the proposed machine, like the multiaxial fatigue machine shown in Patent [20], allows testing with complex loading cycles.

This work refers to the planning, development, construction, and testing of a multiaxial fatigue machine, low cost, easy to control, and operate in relation to commercial multiaxial fatigue machines. The main objective of the machine is evaluating the behavior and obtain experimental parameters of the main models of multiaxial fatigue for aluminum alloys developed at the Federal University of Pará, which is one of the main lines of engineering research at this university.

2. MATERIALS AND METHODS

The construction of the multiaxial fatigue machine described here was based on three main items, 2.1 Four-bar mechanism, 2.2 Load cell, and 2.3 Control. The Schematic of the multiaxial fatigue machine is shown in Figure 1(a) and Figure 1(b) shows the local and geometry of specimens used in the tests. The multiaxial fatigue machine allows for any specimen geometry that is within the defined length between the two support to fix specimens and maximum load of motors.

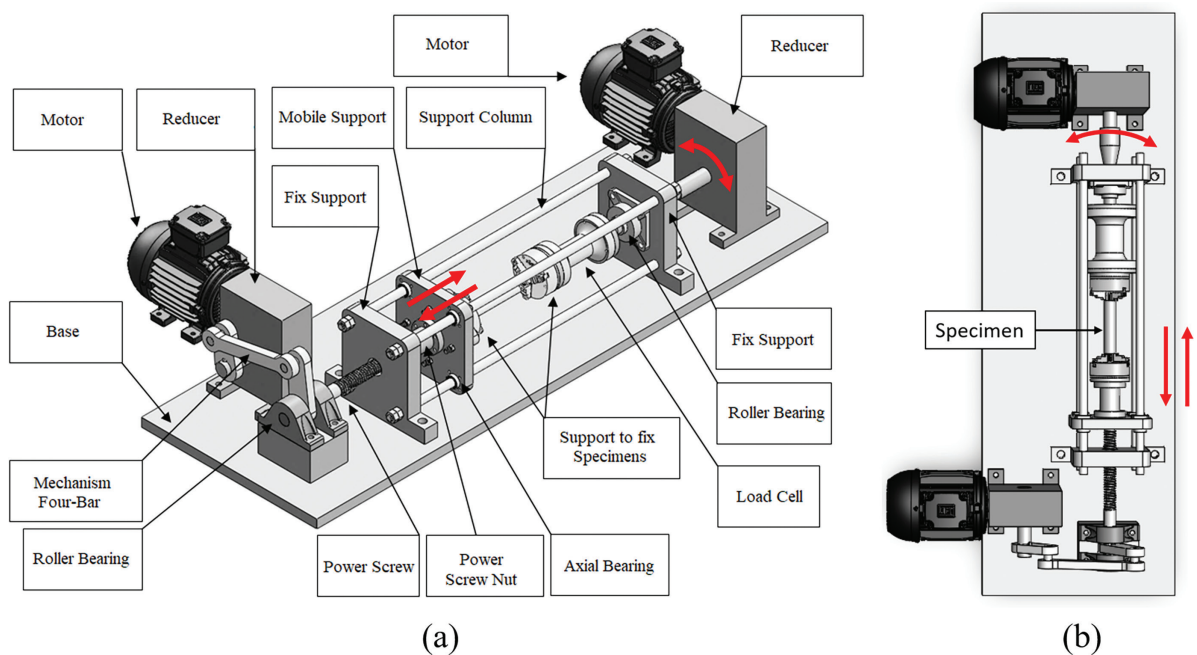


Figure 1: Multiaxial fatigue machine. (a) Schematic of the multiaxial fatigue machine and (b) specimen.

2.1. Four-bar mechanism

Among the many possible configurations for mechanisms, the four-bar mechanism with pin joints stands out, as it is extremely versatile in terms of types of movements, simple modeling and construction. The use of the mechanism to which this work prevents premature wear of the gear reducer, which applies tension and compression loads because the application of alternating axial loads would need to alternate several times the direction of rotation of the motor with high loads, which is harmful to the equipment. As an advantage of this mechanism, the motor can rotate continuously in a single direction because the change in the rotation of the power screw (the output shaft of the mechanism) is controlled by the four-bar mechanism, coupled to the output of the gear motor, shown in Figure 1. For the torsion load was not build one mechanism. However, based on the good results verified for the axial load side, a similar mechanism should be installed in the future for the torque application side. Figure 2 shows the schematic representation of the four-bar mechanism for transmitting, where the numbers mean the linkage number and θ is the angle of said linkage.

According to the Grashof Criterion, if the sum of the lengths of the smallest and largest links is less than the sum of the lengths of the remaining links, the assembly obeys the Grashof condition and then, at least one of the links is capable of performing a complete rotation around the reference link. If the Grashof relation is obeyed, the assembly is known as a Class I kinematic chain; it will have as movement possibilities the type crank follower, double crank, and double Grashof follower.

Due to the design conditions and dimensions, it was chosen to work with class I, because it is easy to control the position and speed of the gearmotor through one velocity set-point, in addition to the fact that it preserves the gearmotor from mechanical and electrical voltage due to rotation inversion. For the Grashof condition to be equal to the first condition, the four-bar mechanism was designed with a crank link (L_2), of 80 mm, connected to the shaft of the reducer (O_2) and which is free to make a complete and continuous turning. The coupler link (L_3), with 220 mm, connects the crank link to the follower link (L_4); it will describe a general plane movement. The follower link, 120 mm long, is positioned between two bearings and connected to the power screw shaft (O_4). This link will not be free to make a complete turning but will allow the reversal of rotation on the screw shaft, allowing the movement of back and forward in the nut screwed into the power screw, and with this, the tension and compressive axial loads can be applied to the sample coupon to be tested in the multiaxial fatigue machine, as shown in Figure 1. The fixed link is the imaginary link between O_2 and O_4 . The angle θ_3 is the angle formed by link L_2 and link L_3 . Table 1 shows the links classification and length of the links of the mechanism four-bar.

The tension and compression mechanism were designed with two interconnected and dependent mechanisms. The first is the four-bar mechanism, and the second is the power screw with its nut, which has one degree of freedom, and the power screw and power nut have a pitch of 6 mm. The second mechanism, due to its simplicity, does not require further details regarding its kinetic or dynamic analysis.

From the analysis of the positions of the four-bar mechanism, with θ_2 as input, it was possible to determine the movement of the power screw through the follower link movement, as shown in Figure 3.

In order to determine the forces in all joints and supports, as well as the torque required to move the mechanism, a dynamic analysis of the mechanism was made, taking into account the weight force of all links described in Figure 4.

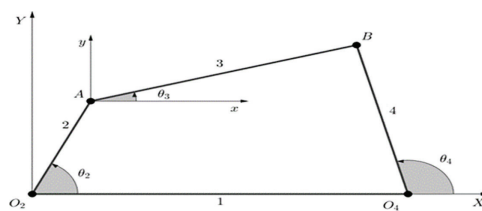


Figure 2: Schematic representation of the four-bar mechanism.

Table 1: Classification and length of links.

LINK	CLASSIFICATION	LENGTH (mm)
L_1	Fix Link	217.5
L_2	Crank Link	80.0
L_3	Coupler Link	220.0
L_4	Follower Link	120.0

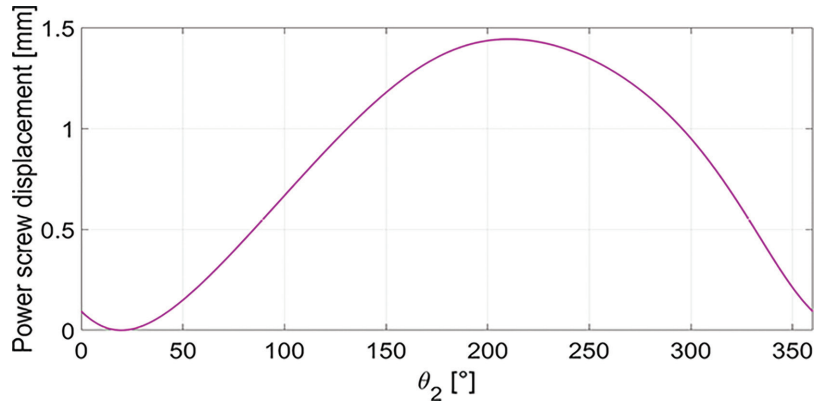


Figure 3: Graph of screw displacement as a function of angular variation of the crank link.

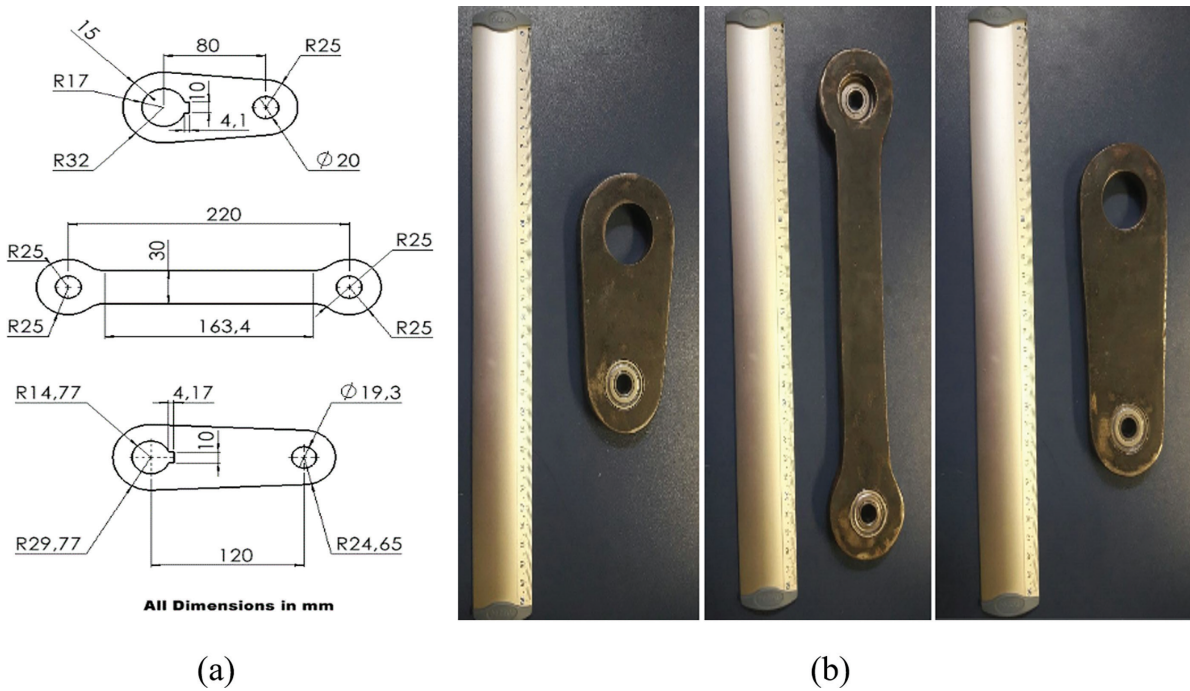


Figure 4: Design of the links. (a) Link dimensions and (b) link build in steel 1020 Steel SAE 1020.

The directions taken as positive for the analysis are: right on the x-axis; up on the y-axis and to the sum of momentum will be counterclockwise, as shown in Figure 5.

The mechanism four-bar was described dynamically on the matrix of Equation (1), generated through dynamic analysis, and with the input data contained in Table 2, considering a torque of output equal to $T_2 = 100 \text{ N.m}$ with a frequency of 1.15 Hz to perform tests in an aluminum test body of 12 mm diameter (estimated $T_4 \approx 70 \text{ N.m}$).

$$\begin{bmatrix}
 1 & 0 & 1 & 0 & 0 & 0 & 0 & 0 & 0 & 0 \\
 0 & 1 & 0 & 1 & 0 & 0 & 0 & 0 & 0 & 0 \\
 -R_{12,y} & R_{12,x} & -R_{32,y} & R_{32,x} & 0 & 0 & 0 & 0 & 1 & 0 \\
 0 & 0 & -1 & 0 & 1 & 0 & 0 & 0 & 0 & 0 \\
 0 & 0 & 0 & -1 & 0 & 1 & 0 & 0 & 0 & 0 \\
 0 & 0 & R_{23,y} & -R_{23,x} & -R_{43,x} & R_{43,x} & 0 & 0 & 0 & 0 \\
 0 & 0 & 0 & 0 & -1 & 0 & 1 & 0 & 0 & 0 \\
 0 & 0 & 0 & 0 & 0 & -1 & 0 & 1 & 0 & 0 \\
 0 & 0 & 0 & 0 & R_{34,y} & -R_{34,x} & -R_{14,y} & R_{14,x} & 0 & 0
 \end{bmatrix}
 \cdot
 \begin{bmatrix}
 F_{12,x} \\
 F_{12,y} \\
 F_{32,x} \\
 F_{32,y} \\
 F_{43,x} \\
 F_{43,y} \\
 F_{14,x} \\
 F_{14,y} \\
 T_2
 \end{bmatrix}
 =
 \begin{bmatrix}
 m_2 a_{CG_{2x}} \\
 m_2 a_{CG_{2y}} + P_2 \\
 I_{CG_2} \alpha_2 \\
 m_3 a_{CG_{3x}} \\
 m_3 a_{CG_{3y}} + P_3 \\
 I_{CG_3} \alpha_3 \\
 m_4 a_{CG_{4x}} \\
 m_4 a_{CG_{4y}} + P_4 \\
 I_{CG_4} \alpha_4 - T_4
 \end{bmatrix}
 \quad (1)$$

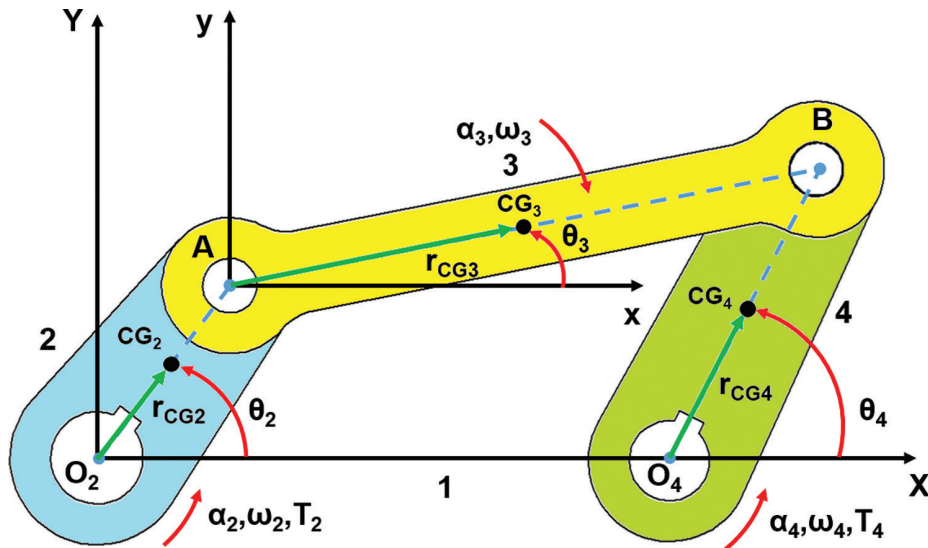


Figure 5: Dynamic analysis of a four-bar mechanism.

Table 2: Mass properties of the links.

COMPONENT	MATERIAL	MASS (kg)	MOMENT OF INERTIA (g.m ²)	CENTER OF MASS (mm)
L ₂	Steel SAE 1020	0.934	1.482	36.71
L ₃	Steel SAE 1020	1.347	8.650	110.00
L ₄	Steel SAE 1020	1.243	2.908	57.33

Table 3: Properties of the links and fatigue safety factor.

COMPONENT	MISES STRESS (MPa)		SF
	MEAN (σ_m)	ALTERNATING (σ_a)	
L ₂	0.8	9.9	10.3
L ₃	0.1	2.6	39.5
L ₄	2.2	14.6	6.8

Where R is the distance between the points on an axis, F is the force applied between the points on an axis, m is the mass of the corresponding link, a_{CG} is the linear acceleration of the center of gravity of the corresponding bar on an axis, I is the moment of inertia, α is the angular acceleration of the corresponding link, P is the corresponding weight force of each bar, and T is the torque applied to the corresponding link [21].

With the dynamic analysis it was possible to identify the variation of stress throughout a crank bar cycle, and then the stress analysis was made in the critical sections of each link with the consideration of fatigue failure, as shown in Table 3. In Table 3 are shown the maximum Von Mises stresses with mean loads and alternating loads for all links. It was considered the material steel SAE 1020, has 380 MPa of ultimate strength stress (S_{ut}), 190 MPa of fatigue limit stress (S_e), in addition, loading correction factor equal to 1.000 (C_L), size correction factor equal to 0.777 (C_S), surface correction factor equal to 0.934 (C_F), temperature correction factor equal to 1.000 (C_T) and reliability correction factor equal to 0.753 (C_R), finally obtaining the fatigue limit stress by $S_e = S_e' C_L C_S C_F C_T C_R = 103.8$ MPa. The safety factor (SF) for the L₂, L₃ and L₄ components was based on Goodman criteria [1], which uses the applied mean stress (σ_m) and alternating stress (σ_a), with S_{ut} and S_e , as shown in Equation (2). The safety factor for fatigue (SF) for the L₂, L₃ and L₄ components are shown in Table 3.

$$SF = \frac{1}{\left(\frac{\sigma_m}{S_{ut}}\right) + \left(\frac{\sigma_a}{S_e}\right)} \quad (2)$$

Figure 6(a) shows the power screw and nut design, whereas Figure 6(b) shows the manufactured power screw and nut. The power screw followed the ACME standard for an external diameter of 30 mm and a thread

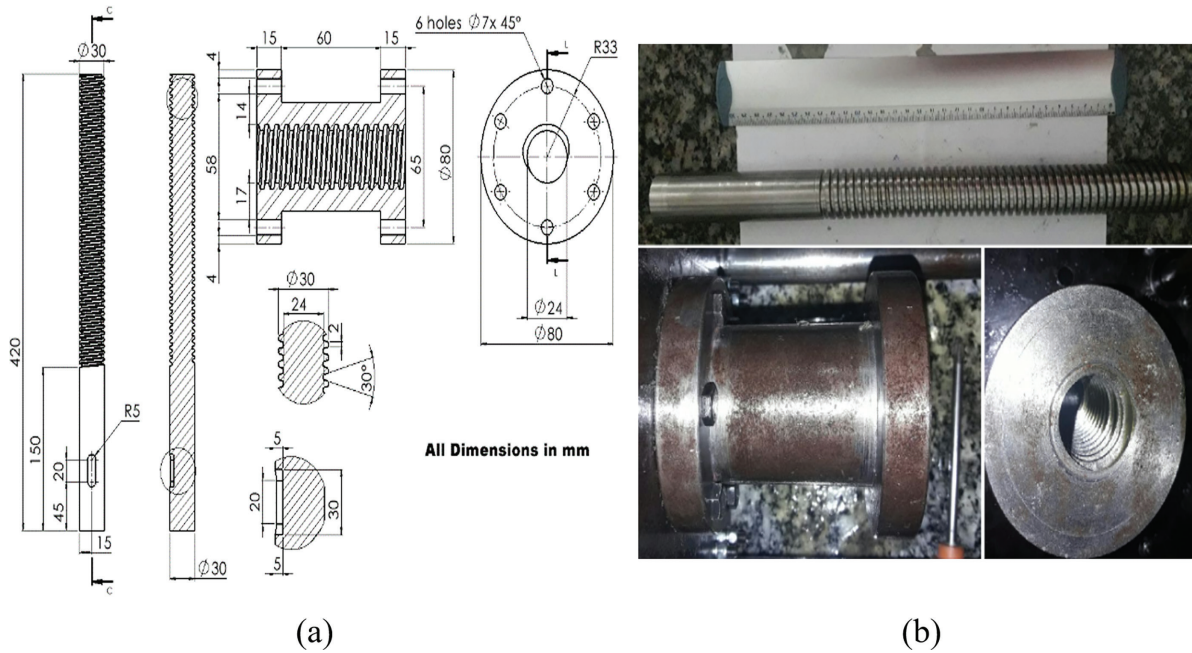


Figure 6: Power screw design, (a) power screw dimensions and (b) power screw machined.

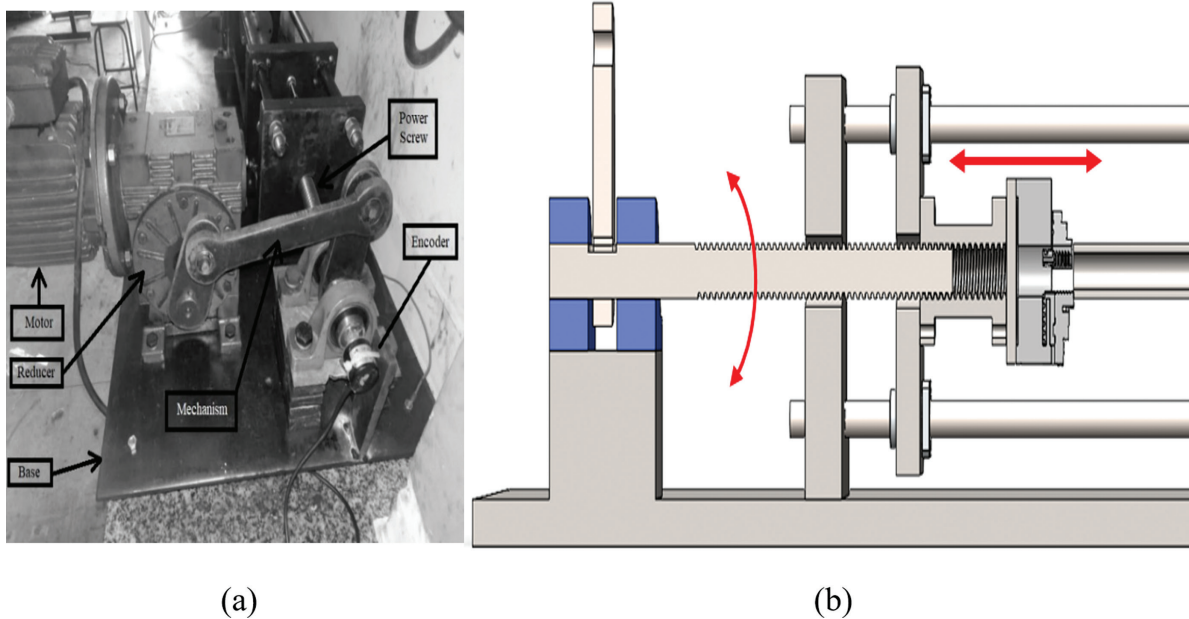


Figure 7: Four-bar mechanism mounted. (a) mounted mechanism and (b) details mechanism.

pitch of 6 mm. In the tests with structural materials, the alternating spins of the power screw are a few degrees, resulting in small displacements. The power screw was machined from a circular bar of SAE 304 stainless steel, 30 mm in diameter and 420 mm long, while the power nut was machined from a circular bar of SAE 1020 steel, 100 mm in diameter and 100 mm long.

The mounted mechanism is shown in Figure 7(a) and the detail of the mechanism is shown in Figure 7(b).

2.2. Load cell

The casting and machining process of the load cell was designed for an alloy of Aluminum, Zirconium, and Magnesium (Al-Zr-Mg), materials available for use, but to find a good relationship between mechanical properties and use of the load cell, a study was carried out with the alloys: Al-0.2%Zr and Al-0.2%Zr-2%Mg. The possibility of studying the influence of two types of heat treatment was also studied: T8 and T9. The T8 heat treatment is characterized by the process of solubilizing the alloy, cold deforming it and artificially aging it,

Table 4: Summarized information of Al-0.2%Zr (Alloy A) and Al-0.2%Zr-2%Mg (Alloy B) alloys without heat treatment (STT) and with heat treatments T8 and T9.

ALLOY	TENSION TEST					
	STT		T8		T9	
	UTS (MPa)	YIELD STRENGTH (MPa)	UTS (MPa)	YIELD STRENGTH (MPa)	LRT (MPa)	YIELD STRENGTH (MPa)
A	171.06	167.64	164.13	151.02	160.52	152.08
B	355.31	342.71	347.82	298.50	322.57	223.52

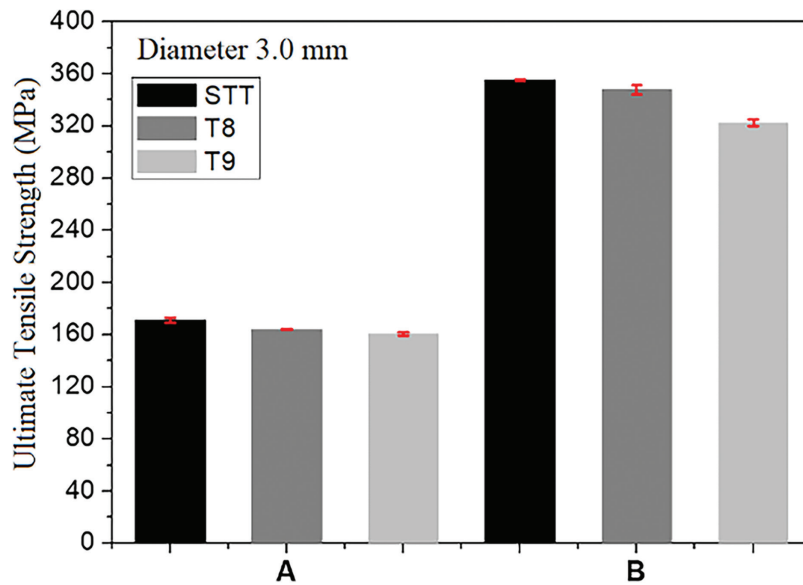


Figure 8: Al-0.2%Zr (Alloy A) and Al-0.2%Zr-2%Mg (Alloy B) alloys without heat treatment (STT) and with heat treatments T8 and T9.

while the T9 heat treatment is characterized by the process of solubilizing the alloy, artificially aging it and cold deforming it. The results obtained from Al-0.2%Zr (Alloy A) and Al-0.2%Zr-2%Mg (Alloy B) alloys without heat treatment (STT) and with heat treatments T8 and T9 are shown in Figure 8 and summarized in Table 4.

When analyzing the untreated alloys (STT), it is noted that adding Mg caused an increase in the tension strength limit in alloy B, twice the result presented by alloy A. In the case of mechanical strength, the highest amount of solute present in this alloy caused greater solid solution hardening and, associated with the applied cold work, caused a significant increase in its tension strength limit. When evaluating the alloys after heat treatments T8 and T9, it is noted that losses occur in the limit of tension strength and yield stress for both alloys. For alloy A, the losses are approximately 4% in the T8 treatment and 6% in the T9 treatment. In the case of alloy B, the losses are approximately 2% in the T8 treatment and 9% in the T9 treatment. It is concluded that the highest limit of tension strength and yield stress was observed for the cast alloy, and the treatments T8 and T9 were inefficient in promoting strength increase of the alloys. Therefore, it was decided not to perform these heat treatments on the material, opting for alloy A to construct the load cell. The mechanical design for the load cell was based on the one used by SANCHEZ [19], and the cell designed for this work used an aluminum alloy Zirconium and Magnesium (Al-0.2%Zr-2%Mg).

The information on the loads applied to the specimens during the tests will be given by the load cell instrumented with electrical resistance strain gauges, as shown in Figure 9. After instrumentation, the load cell was calibrated to allow the conversion of the strain values into load, axial, and torque.

The parameters used in the design and evaluation of the cell are shown in Table 5, Table 6, and Table 7.

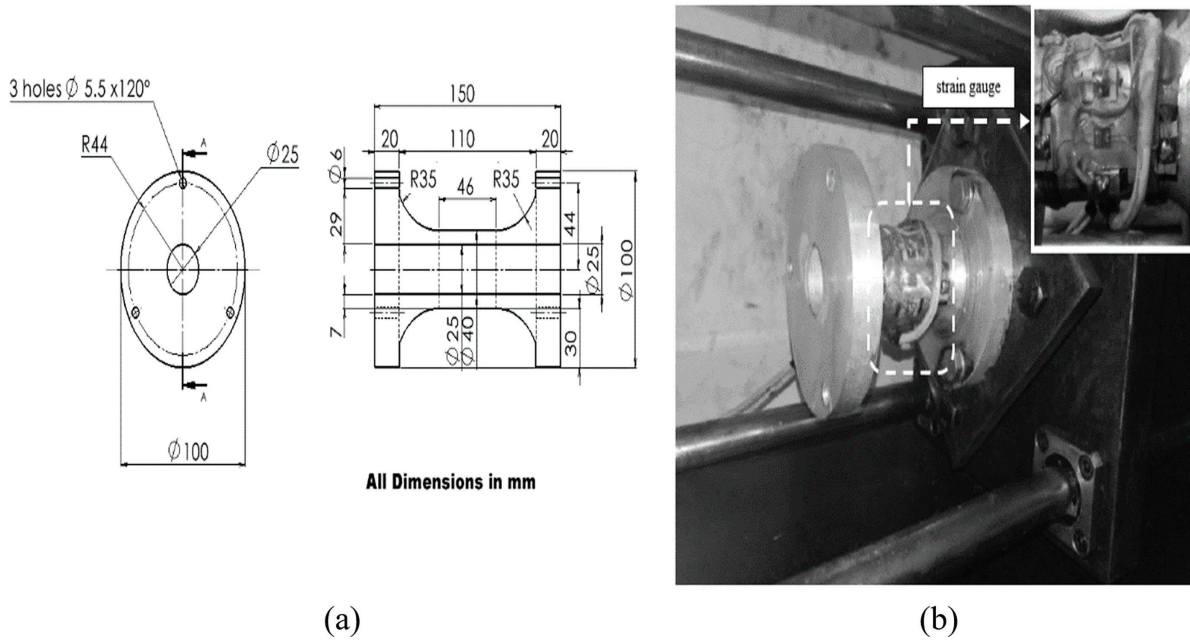


Figure 9: Load cell design, (a) load cell of dimensions, and (b) load cell manufactured.

Table 5: Aluminum properties used for load cell design.

Modulus of elasticity	68 GPa
Modulus of shear	26 GPa
Poisson's coefficient	0.33

Table 6: Data used for the construction of the load cell.

Maximum axial load $\sigma_{axial_{max}}$	10 kN
Maximum torsional load	15 N.m
External diameter	40 mm (bonding zone)
Internal diameter	25.4 mm

Table 7: Stresses and strains calculated for maximum load.

	MAXIMUM AXIAL LOAD	MAXIMUM TORSIONAL LOAD	COMBINATION OF LOAD
	10 kN	15 N.m	10 kN e 15 N.m
Stress (MPa)	13.33	1.43	13.56
Strain ($\mu\text{m/m}$)	196	56	199

To calculate the load cell fatigue safety factor, the Findley method was used because it works with macroscopically elastic proportional and non-proportional stresses [1]. The Findley method was used, as a conservative design was sought for multiaxial fatigue, since the Findley method is applicable for non-proportional loads, and therefore they are the worst scenario thought for the load cell in the experimental tests. Its central idea is the assumption that the fatigue crack originates in the critical plane of the critical point of the part, in which the damage is maximum. The fatigue damage is caused by the combination of the shear stress amplitude in the critical plane $\tau(\theta_{critical})$ and the normal stress in the plane perpendicular to it $\sigma_{\perp}(\theta_{critical})$. Thus, cracking is expected in a direction $\theta_{critical}$ from the critical point where the combination of these two stresses is maximum, the Equation (3) shown the Findley [1].

$$\tau(\theta_{critical}) + \alpha_{Findley} \sigma_{\perp}(\theta_{critical}) = \beta_{Findley} \quad (3)$$

It was applied for non-proportional loads with a $\pi/2$ lag (higher non-proportionality factor) pulsating and alternating, as performed by VORMWALD *et al.* [22]. The graphs of axial and torsional forces for the pulsating non-proportional case are shown in Figure 10(a) and 10(b). The graphs of axial and torsional forces for the alternating non-proportional case are shown in Figure 10(c) and 10(d).

The stress plane angle is then varied, and the stresses in the analysis plane are summed up to find the largest Findley parameter (β_{Findley}), which is the sum of the shear stress amplitude and the normal stress in the plane of analysis is an perpendicular plane multiplied by the Findley factor (considered here $\alpha_{\text{Findley}} = 0.3$) [1]. Figure 11(a) and 11(b) shows the variation of the β_{Findley} parameter with the angular variation in the xy for the plane critical where the parameter is maximized, normal stress σ_y and shear stress τ_{xy} , for the case of pulsating non-proportional loading.

Table 8 presents the values of the fatigue safety factors by the Findley criterion for the load cell, using an estimated Findley limit of 28 MPa.

The found safety factor for the load cell by Findley was 2.9. This safety factor demonstrates that the load cell design is conservative.

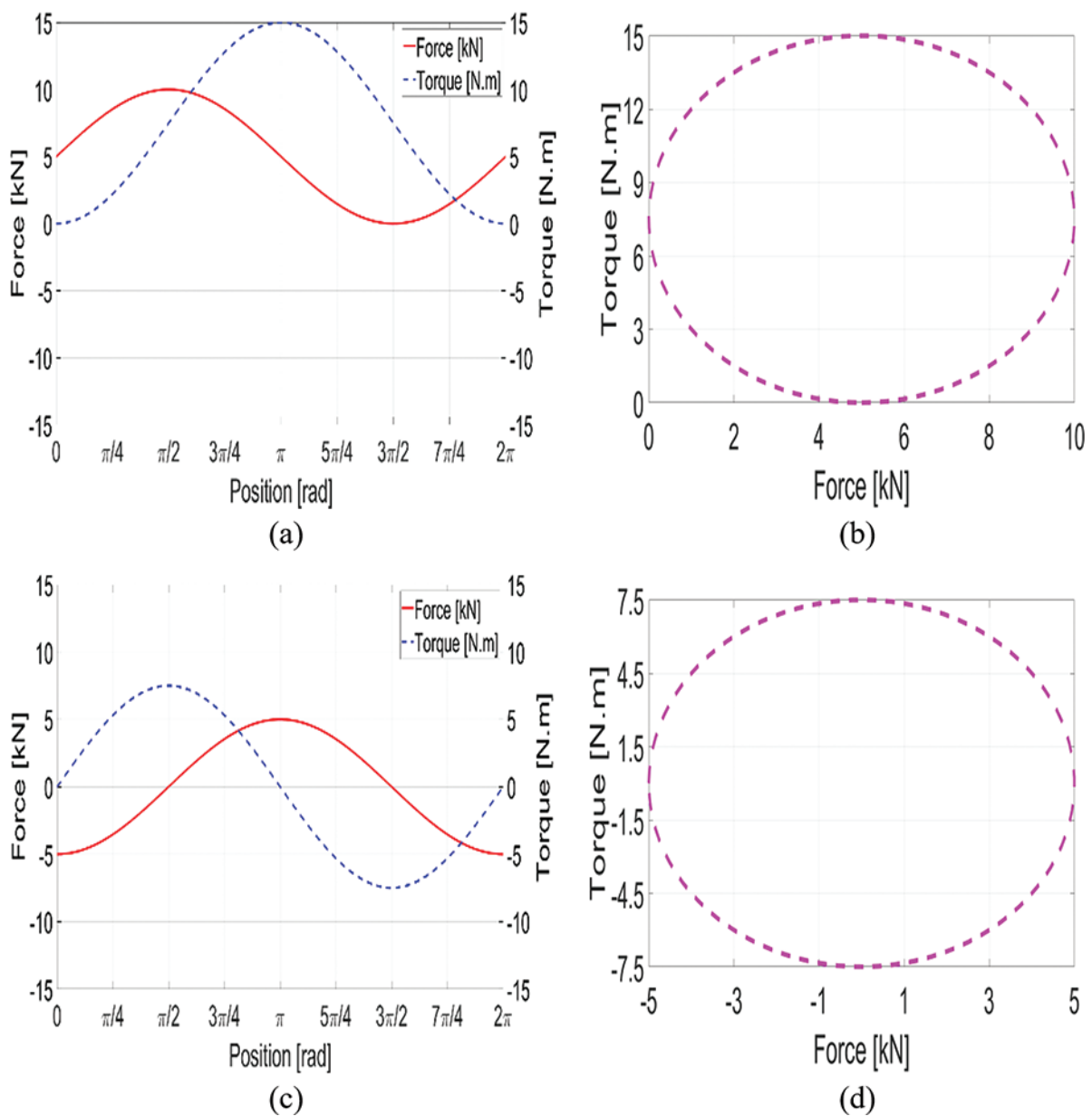


Figure 10: Axial and torsional forces for the pulsating non-proportional case with pulsating and alternating load. (a) pulsating load, (b) pulsating force-torsion load diagram, (c) alternating load and (d) alternating force-torsion load diagram.

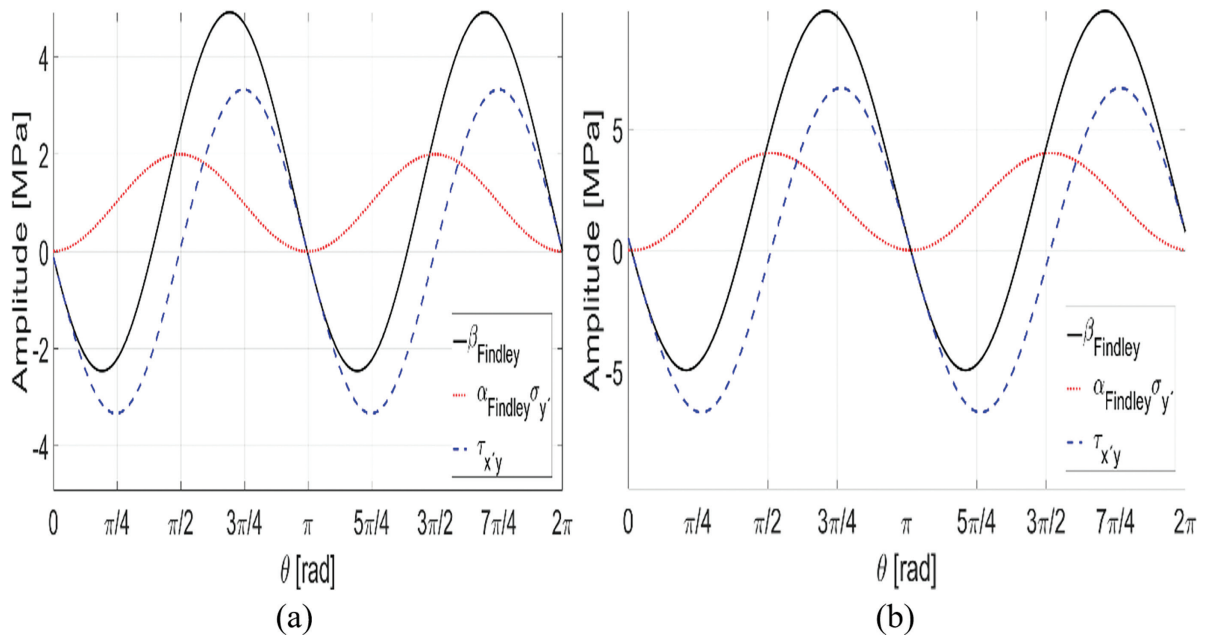


Figure 11: Obtaining the critical plane and the stresses acting on the critical plane: pulsating non-proportional loads.

Table 8: Tension strength limit results.

	NOT PROPORTIONAL, OUT OF PHASE AND PULSATING	NOT PROPORTIONAL, OUT OF PHASE AND ALTERNATE
Factor of safety by Findley	2.9	5.8

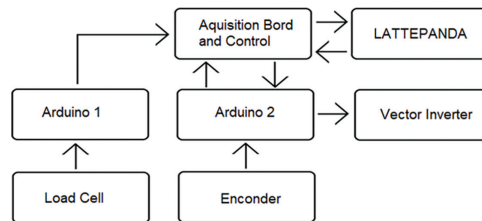


Figure 12: Measurement and control chain.

2.3. Control

The control system is based on the signals obtained from the strain gauges in the full Wheatstone bridge of the load cell since the deformations read by the acquisition system and later converted into voltage will be the reference of the test, allied to the feedback of two position sensors (encoders). Each encoder is positioned at the output of each geared motor; the encoder used is NPN type and has a response of one pulse per degree. The signals coming from the load cell will be read by two HX711 boards, one for each complete bridge (one for tension/compressive stress and the other for torsional stress), which amplified, filtered, and converted the analog signals into digital ones and which are later processed by an Arduino® board (Arduino 1) that will communicate with the LattePanda® board through the USB port. The data is visualized and stored through the graphical interface software installed on the LattePanda®. The encoder signals are sent to another Arduino® board (Arduino 2) and later to LattePanda®, and there is an intermediate board between the Arduino® boards and the LattePanda®, called an acquisition and command board. This board serves as support for the physical connections between boards and the correct powering of the sensors. The software installed on the LattePanda® monitors the loading history and applied loads. The measurement and control blocks are shown in Figure 12.

The DAQ system (Data Acquisition) of the load cell and encoders is shown in Figure 13(a), and the control panel for the multiaxial fatigue machine is shown in Figure 13(b).

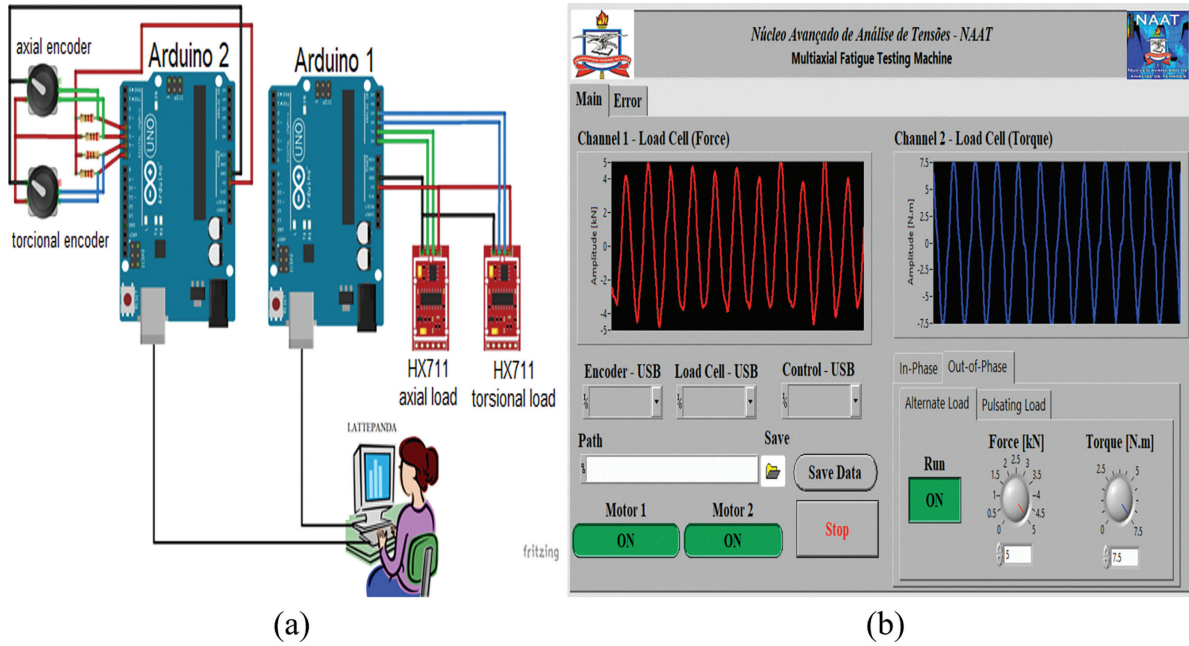


Figure 13: DAQ system and panel control, Figure 13(a) DAQ system of the load cell and encoders and Figure 13(b) panel control of the multiaxial fatigue machine.

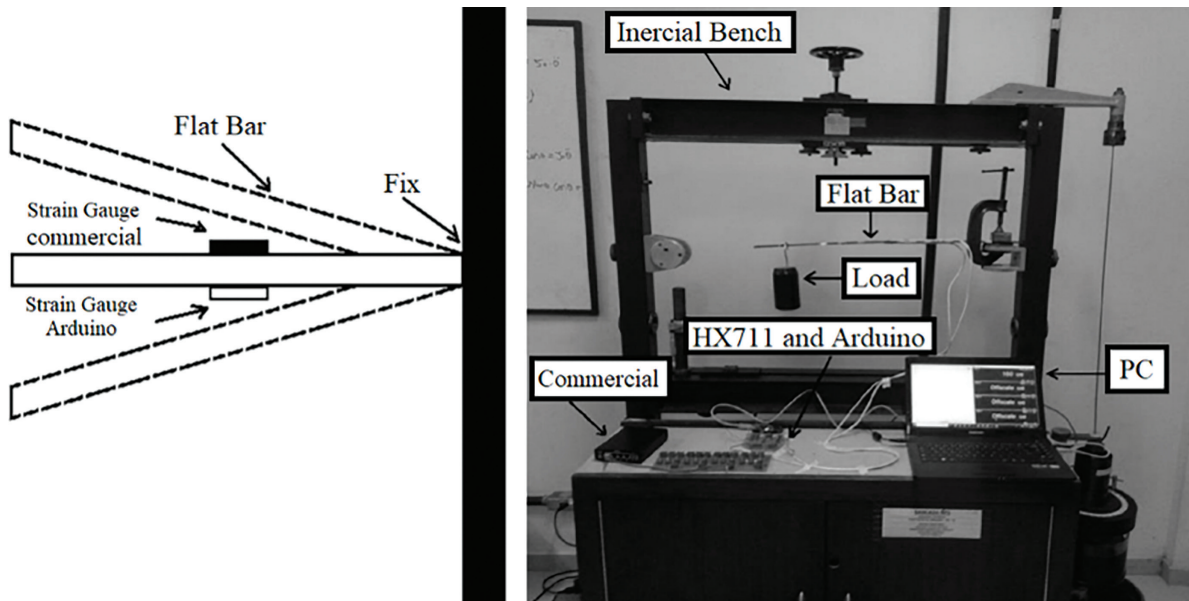


Figure 14: Reading of the extensometers at the same time with the commercial signal acquirer and conditioner and HX711 board with Arduino 1 for comparison and validation of the system.

Before using the data from the load cell, it was validated with two parallel strain gauges on a 500 mm flat metallic bar set in a high rigidity and inertia bench. One strain gauge was glued on the upper face and the other on the lower face. The D4 Data Acquisition Conditioner from Micro-Measurements with sample rate 8 Hz, named commercial, performed the reading of extensometer at the top, and the conditioner and HX711 board with Arduino 1 with 20 Hz, performed the reading of extensometer at the bottom. Figure 14 shows the positioning of the extensometers and the assembled system. The bar is 5 mm thick, 30 mm wide and 50 cm long. Reading of the extensometers at the same time with a commercial signal acquirer and conditioner and HX711 board with Arduino 1 for comparison and validation of the system.

The validation was carried out in two scenarios. The first was a static load scenario, for a constant load application through a known weight at a certain distance on the bar, and the second was the dynamic scenario,

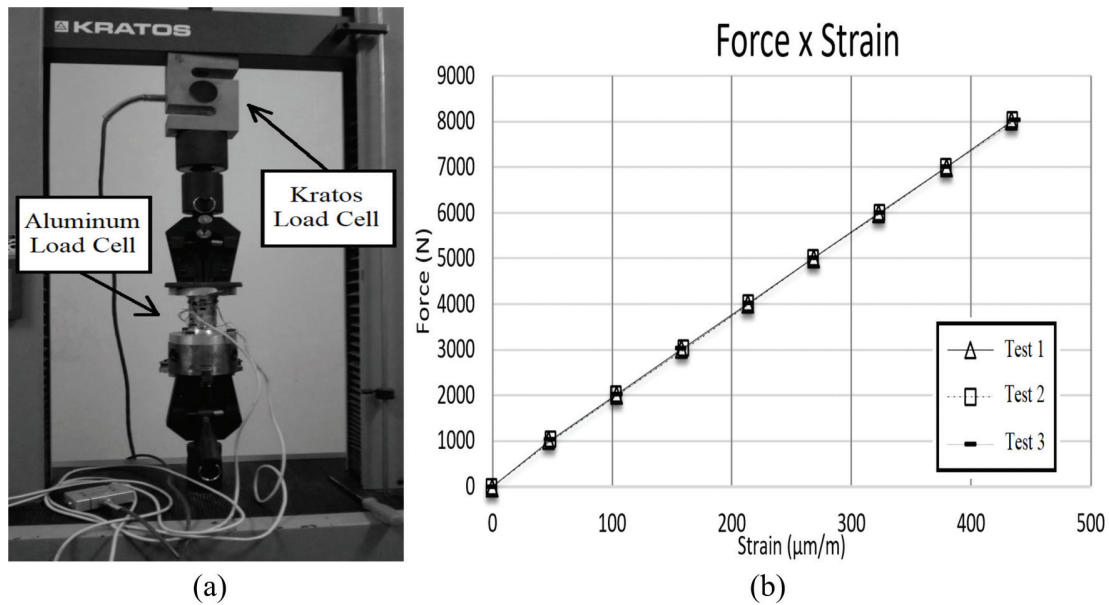


Figure 15: Aluminum load cell calibration, Figure 15(a) aluminum load cell positioned in the tension machine for calibration and Figure 15(b) the results obtained in the tests.

for an impulsive load application. The first one was the static condition, after taking the deformation value, the known weight of 680 g was placed at a distance of 150 mm from the extensometer to obtain the strain read by the extensometers.

A calibration was performed using a Universal Testing Machine (UTM) Kratos model KE 3000MP with a 2000 N load cell, for which three tension tests were carried out with the aid of the already calibrated commercial load cell installed on the machine, where the UTS was configured to apply static loads from 0 to 8000 N, with steps of 1000 N. Figure 15(a) shows the calibration procedure, for axial forces, of the load control system with the cell built with a duly calibrated commercial load cell as a reference. The linearity between the force data from the commercial load cell and the strains read in the strain gauges connected in full bridge attested to the reliability of the manufactured load cell and allowed a correlation constant (gain) between strains read and applied forces, which was placed in the machine load control. Figure 15 (b) shows the graph of the force measured by the commercial load cell \times strain measured in the manufactured aluminum load cell.

Excellent repeatability and linearity can be seen in the three tests, which can attest to the good quality of the instrumentation performed in the load cell and the designed data acquisition equipment. The average of longitudinal strain variations indicated by the cell for each 1000 N was approximately 54 $\mu\text{m/m}$, while the value calculated from the dimensional data and mechanical properties considered was 52 $\mu\text{m/m}$. This represents an approximate error of 4%, which is an acceptable error for this type of experiment, also demonstrating that the designed acquisition equipment works satisfactorily. With the results obtained, it can be seen that the load cell region and the properties considered for the aluminum alloy were consistent, as the analytical and experimental results were very close. A test was also performed to validate the relations of deformations obtained by the torque rosettes with the applied torque, obtaining the most adequate gain for these rosettes. The test consisted of fixing a bar perpendicular to the load cell and placing known weights in different positions on the bar, which generated torque in the plane of the cell. Knowing the torque and knowing the deformation that it should cause in the cell, the gain to be used was defined.

3. RESULTS AND DISCUSSION

In order to test the control system and the methodologies employed, nylon specimens were used, as it is a relatively homogenous material and very easy to machine. In the tests, low loads were used to not significantly plasticize the specimens, which could interfere in the analysis of the load control system. It was performed test with controls for the application out-of-phase loads with 90 phase shift angle (maximum non-proportionality), because they are the cases with greater complexity and challenges from the point of view of mechanical fatigue [1]. When testing the specimen with a pulsating load, loads shown in Figure 16(a) and Figure 16(b) shows

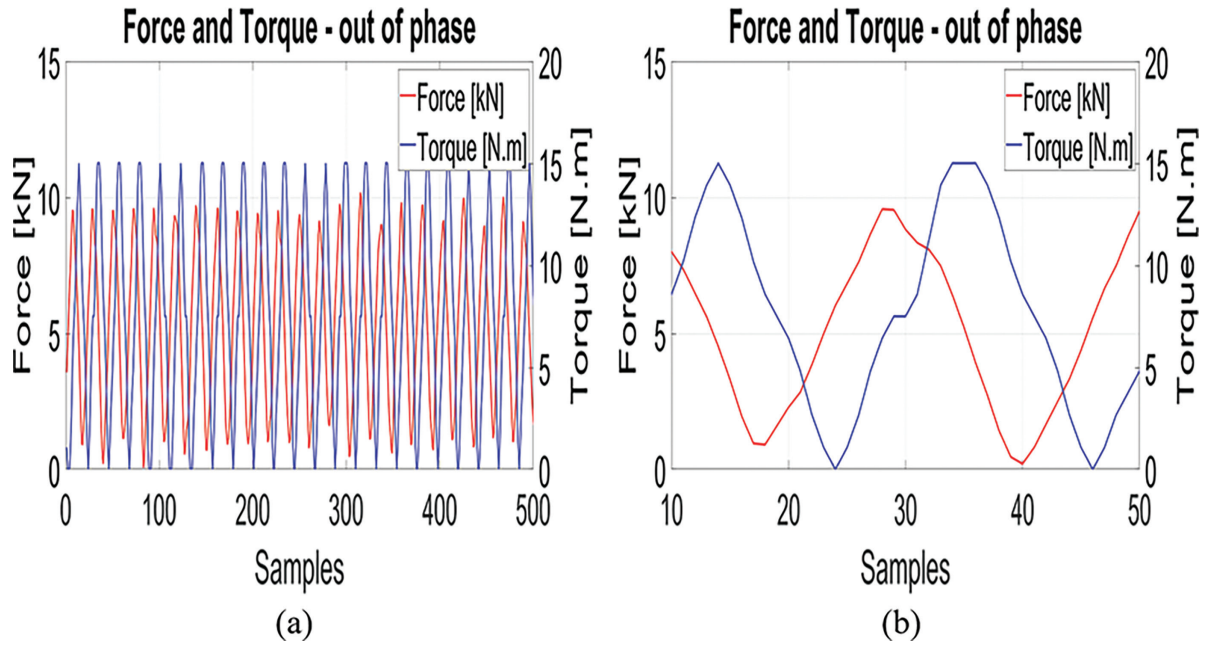


Figure 16: Pulsating loading test. (a) Full test and (b) zoom in on the first two cycles of the test.

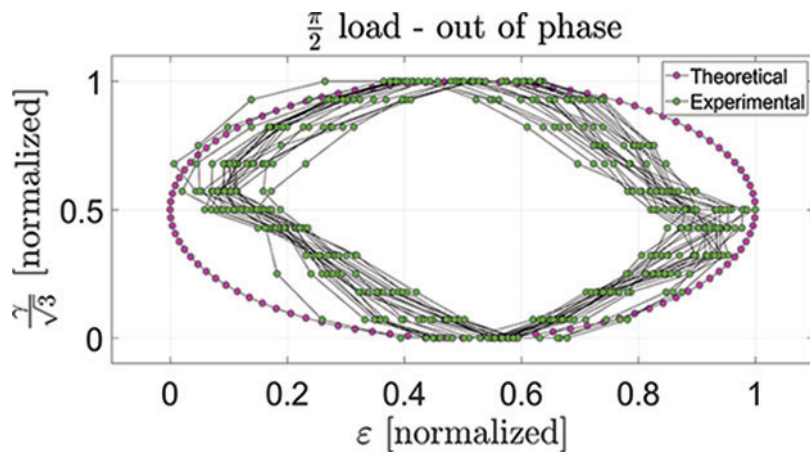


Figure 17: Graph of $\gamma/\sqrt{3} \times \epsilon$ of the test with a pulsating load.

Figure 16(a) zoomed in on the first two cycles, was obtained the graph of shear strain x normal deformations, shown in Figure 17. It is noted that the tension and compression graph does not show peaks due to the movement of the four-bar mechanism and the torsion graph contain backlash due to the inversion of rotation direction [23].

When testing the specimen with alternate loading, loads shown in Figure 18(a) and Figure 18(b) shows Figure 18(a) zoomed in on the first two cycles, was obtained the graph of shear strain x normal deformations, shown in Figure 19. It is noted that the tension and compression graph not shows peaks due to the movement of the four-bar mechanism and the torsion graph contain backlash due to the inversion of rotation direction [23].

It can be observed in Figure 19 the load application for an ideal case of loading out of phase at 90 degrees, as it shows the deformations $\gamma/\sqrt{3} \times \epsilon$ forming an approximately circular shape, similar to the one that appears in [1].

4. CONCLUSION

The work deals with the development and construction of a multiaxial fatigue testing machine with in-phase and out-of-phase torsional and axial load control.

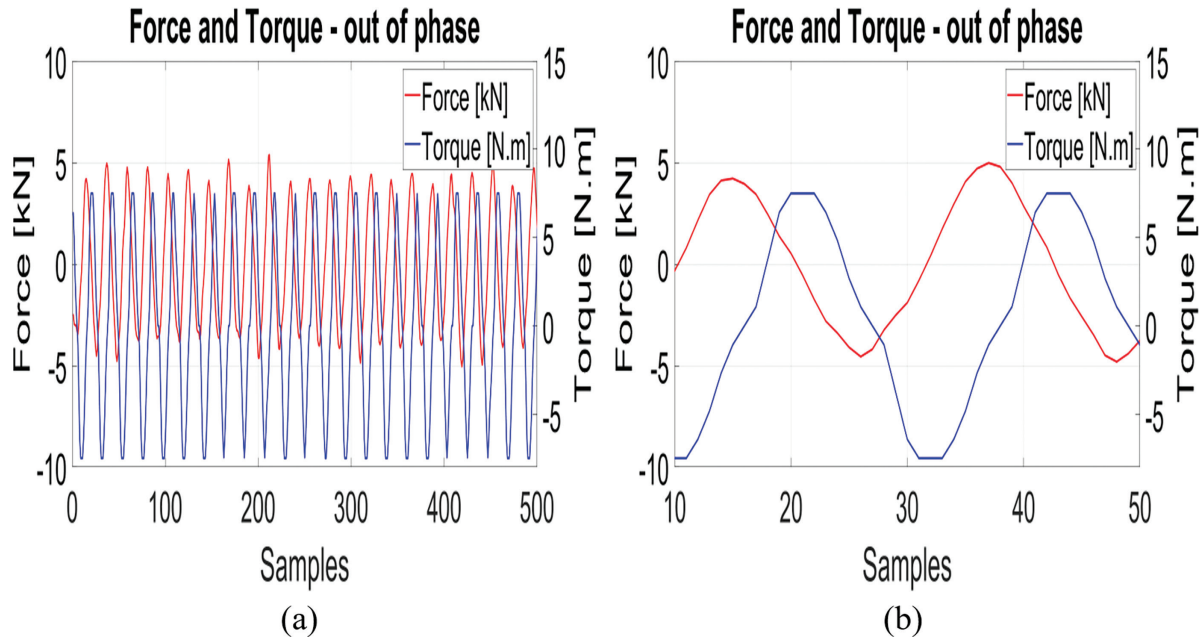


Figure 18: Alternating load test. (a) full test and (b) zoom in on the first two cycles of the test.

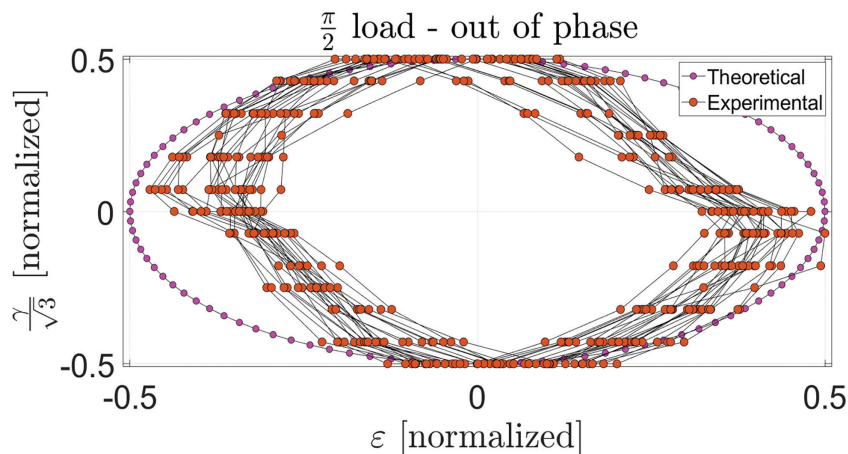


Figure 19: $\gamma/\sqrt{3} \times \epsilon$ graph of the test with alternating load.

The load cell built for the machine was calibrated and proved to be very reliable in providing real-time information to the control system.

A four-bar mechanism for applying tension and compression was used, as it changes its direction of force application without the need for additional electrical commands to the electric motor. Using a transmission system with gears to apply alternating loads can generate deformations in the waveform of the required load, due to the gear clearance (backlash), more precisely at the time of movement reversal. According to LIMA [23], the backlash is more evident for low-frequency movements, and this nonlinear effect is not easy to compensate for classical control laws, as seen in Figure 17, and Figure 19. With the four-bar linkage, the tension and compression gear motor will be less affected by the backlash if it works continuously. However, the torsion reduction motor still has the gear clearance effect, due to the need to reverse the rotation of its shaft to apply pure, pulsating, or variable alternating load. So, one of the machine's future improvements will be the installation of a four-bar linkage that will also be built for the torque application side.

At this moment, the machine is able to apply in-phase and out-of-phase loads, which limits its use for evaluation of specific methods, such as Sines, which can only be applied for proportional loadings, and the Findley method, which can be applied for proportional and non-proportional loadings. It is also emphasized

that the machine allows the application of loads with different factors of non-proportionality, which allows the evaluation of the sensitivity of the materials to this parameter [18]. Thus, the design of the control system proved to be sufficiently adequate to provide the performance of several evaluations in multiaxial fatigue.

5. ACKNOWLEDGMENTS

The authors acknowledge the support provided by the Coordenação de Aperfeiçoamento de Pessoal de Nível Superior - Brazil (CAPES) - Finance Code 001 and the Fundação Amazônia de Amparo a Estudos e Pesquisas (FAPESPA).

6. BIBLIOGRAPHY

- [1] CASTRO, M.A.M., TUPIASSU, J.P.D., *Fatigue design techniques, under real service loads: Vol. I, Vol. II, Vol. III*, Scotts Valley, CA, 95066, USA, Createspace Independent Publishing Platform, 2016.
- [2] LIU, A.F., *Mechanics and mechanisms of fracture: an introduction*, Ohio, ASM International, 2005. doi: <http://dx.doi.org/10.31399/asm.tb.mmmf.9781627083096>.
- [3] BOEIRA, F.D., PINHEIRO, G.S., SPECHT, L.P., *et al.*, “Projeto e implementação de ensaio de fadiga por tração-compressão direta (uniaxial) para avaliação de dano em misturas asfálticas”, *Matéria (Rio de Janeiro)*, v. 23, n. 3, 2018. doi: <http://dx.doi.org/10.1590/s1517-707620180003.0482>
- [4] XIE, J., ZHOU, X., SHE, C., *et al.*, “A review of FMLs performance test methods and index evaluation”, *Revista Matéria*, v. 28, n. 1, pp. e20230006, 2023. doi: <http://dx.doi.org/10.1590/1517-7076-rmat-2023-0006>
- [5] ANDRADE, G.C., “*Fadiga multiaxial policiclica modelagem e simulação*”, M.Sc. Thesis, Universidade de Brasília, Brasília, 2006.
- [6] YANG, J., GONG, Y., JIANG, L., *et al.*, “A multi-axial and high-cycle fatigue life prediction model based on critical plane criterion”, *Journal of Materials Research and Technology*, v. 18, pp. 4549–4563, 2022. doi: <http://dx.doi.org/10.1016/j.jmrt.2022.04.069>.
- [7] KAROLCZUK, A., MACHA, E., “A review of critical plane orientations in multiaxial fatigue failure criteria of metallic materials”, *International Journal of Fracture*, v. 134, n. 3-4, pp. 267–304, 2005. doi: <http://dx.doi.org/10.1007/s10704-005-1088-2>
- [8] FINDLEY, W.N., “A theory for the effect of mean stress on fatigue of metals under combined torsion and axial load or bending”, *Journal of Engineering for Industry*, v. 81, n. 4, pp. 301–305, 1959. doi: <http://dx.doi.org/10.1115/1.4008327>
- [9] GOUGH, H.J., POLLARD, H.V., “The strength of metals under combined alternating stresses”, In: *Proceedings of the Institution of Mechanical Engineers*, pp. 3–103, 1935. doi: http://dx.doi.org/10.1243/PIME_PROC_1935_131_008_02
- [10] GUEST, J.J., “Recent research on combined stress”, In: *Proceedings of the Institution of Automobile Engineers*, pp. 33–72, 1940.
- [11] SINES, G., OHGI, G., “Fatigue criteria under combined stresses or strains”, *Journal of Engineering Materials and Technology*, v. 103, n. 2, pp. 82–90, 1981. doi: <http://dx.doi.org/10.1115/1.3224995>
- [12] WHITE, D.J., CROSSLAND, B., MORRISON, J.L.M., “Effect of hydrostatic pressure on the direct-stress fatigue strength of an alloy steel.”, *Journal of Mechanical Engineering Science*, v. 1, n. 1, pp. 39–49, 1959. doi: http://dx.doi.org/10.1243/JMES_JOUR_1959_001_008_02
- [13] KAKUNO, H., KAWADA, Y., “A new criterion of fatigue strength of a round bar subjected to combined static and repeated bending and torsion”, *Fatigue & Fracture of Engineering Materials & Structures*, v. 2, n. 2, pp. 229–236, 1979. doi: <http://dx.doi.org/10.1111/j.1460-2695.1979.tb01358.x>
- [14] DANG-VAN, K., GRIVEAU, B., MESSAGE, O., *On a new multiaxial fatigue limit criterion: theory and applications, biaxial and multiaxial fatigue*, EGF 3 (Edited by Brown, M.W. and Miller, K.J., Mechanical Engineering Publications, London, pp. 479–496, 1989.
- [15] PAPADOPOULOS, I.V., “A new criterion of fatigue strength for out-of-phase bending and torsion of hard metals”, *International Journal of Fatigue*, v. 16, n. 6, pp. 377–384, 1994. doi: [http://dx.doi.org/10.1016/0142-1123\(94\)90449-9](http://dx.doi.org/10.1016/0142-1123(94)90449-9)
- [16] PAPADOPOULOS, I.V., “High-cycle fatigue criterion applied in biaxial and triaxial out-of-phase stress conditions”, *Fatigue & Fracture of Engineering Materials & Structures*, v. 18, n. 1, pp. 79–91, 2007. doi: <http://dx.doi.org/10.1111/j.1460-2695.1995.tb00143.x>

- [17] PAPADOPOULOS, I.V., “Long life fatigue under multiaxial loading”, *International Journal of Fatigue*, v. 23, n. 10, pp. 839–849, 2001. doi: [http://dx.doi.org/10.1016/S0142-1123\(01\)00059-7](http://dx.doi.org/10.1016/S0142-1123(01)00059-7)
- [18] FATEMI, A., SHAMSAEI, N., “Multiaxial fatigue: an overview and some approximation models for life estimation”, *International Journal of Fatigue*, v. 33, n. 8, pp. 948–958, 2011. doi: <http://dx.doi.org/10.1016/j.ijfatigue.2011.01.003>
- [19] SANCHEZ, E.C.M., “*Desenvolvimento de uma máquina tração-torção de ensaios de fadiga para avaliação de modelos de plasticidade incremental*”, D.Sc. Thesis, Pontifícia Universidade Católica do Rio de Janeiro, Rio de Janeiro, 2014.
- [20] COMAS, A.D.P., *Multiaxial Fatigue Machine: Patent 10883907*, Bucaramanga, CO, Universidad Industrial de Santander, 2021.
- [21] SOUZA, L.P.B., “*Desenvolvimento de uma máquina para ensaios de fadiga multiaxial com controle de carga*”, M.Sc. Thesis, Universidade Federal do Pará, Belem, 2018.
- [22] VORMWALD, M., HOS, Y., FREIRE, J.L., *et al.* “Variable mode-mixity during fatigue cycles - crack tip parameters determined from displacement fields measured by digital image correlation,” *Frattura ed Integrità Strutturale*, v. 11, n. 41, pp. 314–322, 2017. doi: <http://dx.doi.org/10.3221/IGF-ESIS.41.42>
- [23] LIMA, A.S., *Controle por aprendizagem iterativa e controle*, Rio de Janeiro, Universidade Federal do Rio de Janeiro, 2014.